

BLUE PULSE™: ACTIVE ROTOR CONTROL BY TRAILING EDGE FLAPS AT AIRBUS HELICOPTERS

Oliver Dieterich, Antoine Raboutin, Jean-Baptiste Maurice, Peter Konstanzer
AIRBUS HELICOPTERS Deutschland GmbH, Donauwoerth, Germany

Abstract

Ten years ago, AIRBUS HELICOPTERS has opened a new page in active rotor control by performing the first flight of a main rotor system equipped with piezo-driven trailing edge flaps. In 2005, the experimental test bed consisted of a modified BK117 composite airframe and the experimental ADASYS main rotor system labelled according to the underlying research project. In the meantime, the experimental system has been continuously improved in order to close the gap to potential serial solutions in view of airframe, main rotor, actuation and mechatronics. Until today, AIRBUS HELICOPTERS is the only manufacturer in the world performing full scale flight tests with such kind of systems. The related technology is branded by AIRBUS HELICOPTERS as Blue Pulse™.

This paper provides a comprehensive overview on active rotor activities at AIRBUS HELICOPTERS concerning piezo-driven trailing edge flaps. Main topics are the presentation of flight test results and underlying flight physics for major secondary control tasks. Future development challenges are identified to be less on realization by design and proof-of-demonstration for both hardware and control algorithms but more on maturing the underlying concepts in view of potential customer applications.

1. INTRODUCTION

AIRBUS HELICOPTERS is the only organization flying full scale demonstrators of active trailing edge flaps beginning with the ADASYS rotor on an experimental BK117 airframe, [1, 2, 3]. The active trailing edge flaps (TEF) serve hereby as dedicated device for various secondary flight control tasks asking for high frequency control inputs beyond the classical 1/rev by primary control.



Figure 1: ADASYS demonstrator (2006)

In 2009 a new demonstrator based on the serial EC145 airframe performed its first flight (Figure 2) equipped with the existing ADASYS rotor system and new cutting edge digital amplifier and power generation units, Figure 2. This EC145 demonstrator successfully supported the consolidation of gained expertise but also the development of new

functionalities such as in-flight tracking and stability enhancement presented in this paper. The modular controller designs for the different secondary flight control tasks allow maximum flexibility: The controllers – either frequency-domain or time-domain – can be exchanged or combined easily without affecting the TEF control framework architecture. Related flight tests demonstrating the multifunctional concept of active trailing edge flaps have gathered:

- Vibration suppression – now using airframe sensors instead of rotor load sensors
- BVI noise cancellation
- In-flight tracking by feeding back 1/rev or (1&2)/rev airframe accelerations on TEFs
- Lead-lag stability enhancement by feeding back main rotor lag moments on TEFs

These research activities of AIRBUS HELICOPTERS under the label Blue Pulse are one of the main technological columns of the Bluecopter initiative [4] – another complementary one being the Blue Edge design featuring advanced main rotor blade plan-forms, see [5].

The approach getting closer to serial applications is clearly visible in the layout of the experimental EC145 rotorcraft where the hub mounted components compartment now fits below the hub cap thanks to miniaturization of power electronics – an activity significantly supported by the corporate research center AGI (Airbus Group Innovations, formerly EADS Innovation Works).



Figure 2: Blue Pulse demonstrator (2009)

This paper addresses main achievements of the flight test campaigns performed between 2009 and 2011 on a demonstrator configuration consisting of the ADASYS active rotor associated with advanced power electronics architecture and the EC145 airframe. Linked to these tests, AIRBUS HELICOPTERS has achieved two more world premieres by demonstrating in flight two new functions: lead-lag stability enhancement and automatic in-flight tracking.

2. VIBRATION REDUCTION

Vibration reduction by active rotor systems dates back to the early roots of HHC using fast swashplate control inputs for counteracting vibratory loads or vibrations [6]. Different to other IBC approaches in the rotorcraft community in the past, AIRBUS HELICOPTERS relies on vibration control algorithms in the time domain and not in the frequency domain [7] hereby taking advantage of modern system control theories up to the H^∞ framework successfully tested in flight [8].

The vibration suppression function based on time domain disturbance rejection has performed additional evolution steps. The main improvement of the vibration suppression consists in designing the control loop to work with airframe sensors located in the non-rotating frame. By switching from blade strain gauge sensors to accelerometers in the airframe, the system becomes simpler and easier to maintain. Different feedback configurations have been investigated among main gear box and cabin sensors culminating in a successful demonstration in flight. As shown in the block diagram in Figure 3 the feedback loop consists of the following elements:

- Transformation of sensor signals from rotating to non-rotating system using rotor azimuth signal
- Three wash-out filters of second order, with following transfer function:

$$(1) \quad G_W(s) = \frac{2\omega_d \cdot s}{s^2 + 2\omega_d \cdot s + \omega_d^2}$$

- Three servo-compensator providing six state outputs, with following transfer function:

$$(2) \quad G_{SC}(s) = \frac{1}{s^2 + 2\omega_d \zeta \cdot s + \omega_d^2} (1 - s)$$

- Gain matrix calculating collective and cyclic TEF control inputs based on the six compensated signals¹
- Inverse MBC transformation for calculating individual TEF inputs from collective and cyclic TEF signals

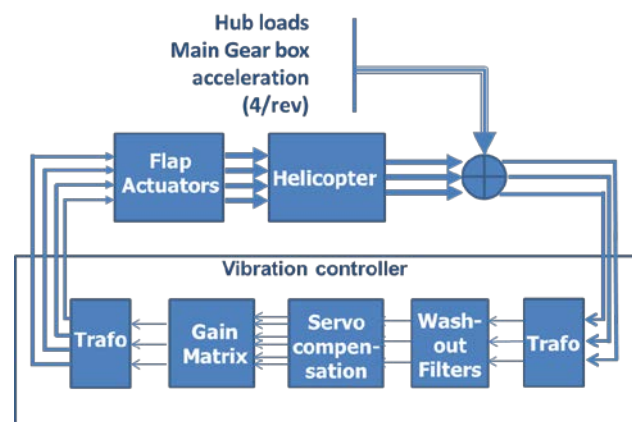


Figure 3: Block diagram of vibration controller

By this design concept, the vibration controller is formulated in the non-rotating system. In case of feedback signals in the airframe e.g. MGB signals, the related transformation block is obsolete and the signals are directly fed into the wash-out filter.

For the new sensors, but also for the new demonstrator, the gain matrix has to be identified. The same methodology presented in [9] for the blade loads has been applied to identify the transfer behavior of eleven main gear box, pilot and co-pilot accelerometers. It consists in open loop actuations of the flaps in a specific flight regime during a flight test, with the three possible actuation schemes 4/rev collective, 4/rev cyclic longitudinal and 4/rev cyclic lateral using multi-blade coordinates.

A particularity of the control feedback on airframe accelerometers is the loss of physical symmetry in the gain matrix. Indeed, with blade load feedback, there is a physical correlation, especially visible in hover, between F_z and θ_{coll} and $\{M_x, M_y\}$ and $\{\theta_{long}, \theta_{lat}\}$ as presented in the Eqs. (3) and (4). Flight testing revealed that the cross terms in Eq. 4 (collective control on moment and cyclic control on

¹ Please note that differential TEF control input is not applied.

thrust force) occurring due to asymmetric inflow conditions in forward flight can be removed without significant degradation of controller performance.

$$(3) \quad Y_{Hub} = R(s).u_{IBC} + d_{Hub}$$

with

$$u_{IBC} = (\theta_{coll}, \theta_{long}, \theta_{lat})^T : input$$

$$Y_{IBC} = (F_x, M_x, M_y)^T : output$$

$$d_{Hub} = (F_x, M_x, M_y)_{Hub}^T : disturbance$$

$$R = fn(G) : Transfer matrix$$

and the gain matrix:

$$(4) \quad G = \begin{bmatrix} g_{coll \rightarrow F_x} & g_{long \rightarrow F_x} & g_{lat \rightarrow F_x} \\ g_{coll \rightarrow M_x} & g_{long \rightarrow M_x} & g_{lat \rightarrow M_x} \\ g_{coll \rightarrow M_y} & g_{long \rightarrow M_y} & g_{lat \rightarrow M_y} \end{bmatrix}$$

However for MGB vibration feedback, the cross terms of the transfer function are all important for the control feedback and the internal structure previously inherent in the gain matrix is lost. Without possibility to assess the importance of matrix entries from physical point of view, the G matrix results in:

$$(5) \quad G = \begin{bmatrix} g_{coll \rightarrow VIB_1} & g_{long \rightarrow VIB_1} & g_{lat \rightarrow VIB_1} \\ g_{coll \rightarrow VIB_2} & g_{long \rightarrow VIB_2} & g_{lat \rightarrow VIB_2} \\ g_{coll \rightarrow VIB_3} & g_{long \rightarrow VIB_3} & g_{lat \rightarrow VIB_3} \end{bmatrix}$$

For the flight demonstration, the investigated vibration sensors were located at pilot and co-pilot seats and on several locations on the MGB. As three sensors were selected for disturbance rejection the best feedback configurations in terms of sensor selection have been identified by using the optimization process presented in [10]. It turned out that a direct feedback of selected cockpit vibration sensors proved not to be efficient from a global point of view as the estimated control effort was very large, leading to vibration increase in other areas of the airframe. Several MIMO and SISO configurations have been successfully flight tested. For the purpose of the paper, only one MIMO and one SISO configuration are presented:

MIMO

- Sensor vector: MGB front left Z, MGB rear left Z, MGB rear right Z
- Control vector (MBC): Collective, cyclic lateral, cyclic longitudinal

SISO

- Sensor signal: MGB front left Z
- Control signal (MBC): Cyclic lateral

As illustrated by Figure 4, both MGB feedback configurations show similar performances at 100 KIAS as the former blade load feedback concept and reduce massively the vibrations up to 80% over all speed conditions. On this graph, the vibration level has been referred to the reference measurement (Blue pulse off) at 120 KIAS. By the transition phase between 20 and 60 knots, and by maximal speed, although the vibration reduction also exceeds 50%, the trend follows the reference measurement. This is due to an authority limitation of the flaps system, as it can be observed on Figure 4. One of the design targets of the next generation Blue Pulse rotor has been to provide more authority in order to bring the vibration level at a constant smooth level over all flight regime without noticing any comfort difference.

A second new feature of the vibration suppression function is the implementation of a time domain output limiter, aiming on limiting the flap actuation angle to desired amplitudes. The related approach consists in scaling of the output vector and in an automatic adaption of damping of the servo compensators. For more details, see [10]. Figure 5 illustrates the 4/rev vibration at pilot seat as function of the flap authority. The vibration has been normed by the reference level measured which control switched off. By the way, it can be observed that the behaviour is quite linear with the available authority, which confirms the hypothesis concerning the helicopter plant. Both the SISO and the MIMO configuration demonstrate very good performances over authority, similar to the blade load MIMO labelled Fz-Mx-My in the figures.

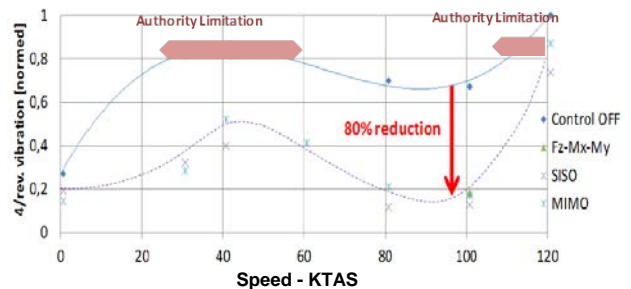


Figure 4: Normalized 4/rev pilot vibration in Z: Level flight speed sweep², control off and on

Furthermore, the robustness of the vibration suppression function has been validated on an extended flight envelope including all speed ranges, turns, climb, descent, and also transient manoeuvres such as flare. Whereas the transfer behaviour is evaluated on one specific flight regimes, for example level flight 100 knots, this single gain matrix is sufficient to provide stable and efficient control over the whole envelope.

² Scaled with reference vibration (system off) at 120kias

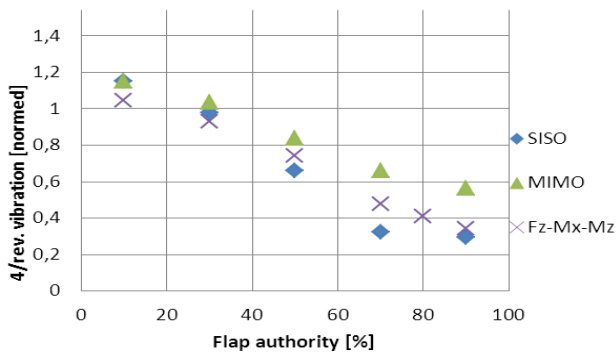


Figure 5: Normalized pilot vibration in Z: Flap authority investigation³ for different controllers

No gain scheduling is necessary to get optimal performances. The disturbance rejection control can deal with variation of transfer behaviour and actuate the flaps with adequate phases and amplitudes, which has been demonstrated in flight.

3. IN-FLIGHT TRACKING

In order to reduce time and costs during production and to avoid or at least reduce related serial test flights automated rotor tracking is on top of the wish-list of rotorcraft industry. In addition for active rotor systems, dissimilarities leading to different blade tip paths might not be only due to non-avoidable tolerances in rotor manufacturing and assembly as for the passive rotors but also due to differences in the characteristics of the actuation units thus increasing the challenges of adequately tracked main rotor systems.

For conventional main rotor systems, different means are typically available for blade tracking which are pitch rod length adjustment and the slight bending of tabs especially foreseen for tracking purposes. These means act different in hover and forward flight allowing to identify a good compromise between different flight states. In case of the TEF rotors, the function of the tabs can be taken over the TEFs applying a small amplitude constant offset.

First AIRBUS HELICOPTERS attempts for the function of in-flight tracking date back to 1990s with investigations in co-operation with ZF by applying hydraulic pitch links of low authority. This research approach later evolved to the highly successive BO105 IBC activities demonstrating significant hub load and BVI noise reduction in flight, [11].

In cooperation with IFR University Stuttgart, AIRBUS HELICOPTERS Deutschland has successfully demonstrated in-flight tracking by online adaptation of quasi-static flap actuation using 1/rev and 2/rev MGB vibration feedback. Thus the tracking control

task in its pure sense – ensuring the blades flying on the same paths leading to a geometric control objective and the non-answered question of suitable sensors in flight – was replaced by the approach of minimizing MGB vibrations with respect to rotor harmonics caused by blade dissimilarities. In fact, main purpose of main rotor blade tracking is to increase comfort for crew and passengers by reducing the related vibration contributions. A thorough description of the control design and concepts is developed in [12, 13].

From a general view, dissimilarities among the rotor blades can cause rotor imbalances further leading to increased vibratory forces at the rotor hub as well as to increased vibration at the gear box and in the cabin of the rotorcraft. The reduction of these unsteady additional loads, mainly occurring at the frequencies 1/rev and 2/rev, can be achieved by steady control inputs to the TEF system as the blade dissimilarities they result from are constant in the rotating system. Thus, it is a natural choice to apply a relaxed HHC algorithm, see equations below – but with specific treatment of the underlying transfer matrix approach (TMA) as a challenging issue by this control concept is the rank deficient transfer matrix $T_{1,2/rev}$ in case of perfectly similar actuation performance of the blades or a highly ill-conditioned matrix in the real world considering slightly different actuators.

$$(6) \quad T_{1,2/rev} = \begin{bmatrix} t_{1,1} & \dots & t_{1,4} \\ \vdots & \ddots & \vdots \\ t_{1,12} & \dots & t_{1,12} \end{bmatrix} = \begin{bmatrix} T_{1/rev} \\ T_{2/rev} \end{bmatrix}$$

$$(7) \quad y_{1/rev;2/rev}^c = T_{1,2/rev} u + y_{1/rev;2/rev}^0$$

In this approach the vector u consists of four elements and identifies the quasi-static control inputs for the blades 1 to 4 while the vector y represents the uncontrolled and controlled gear box vibrations in the frequency domain used for feedback. The matrix $T_{1,2/rev}$ provides the relationship between constant TEF control inputs and 1/rev (and 2/rev) gear box vibrations. Control task of tracking control is to minimize y^c which might lead to slightly different blade paths depending on dissimilar characteristics of the blades.

As already mentioned, two kinds of imperfections have to be taken into account in reality: First, uncontrolled vibrations y^0 are present, asking for in-flight tracking of dissimilar blades in passive operation mode. Second the reaction of flap deflection on gear box vibration is usually slightly different for each blade leading to different entries in the T-matrix as shown in an exemplary manner in Eq. (8) for the relation between the control input

³ Scaled with reference value (system off)

vector and 1/rev vibrations for 60 kts level flight. The circled columns refer to opposite blades and should be identical with a sign change for a perfect behavior. For neighbored blades, a permutation of sine and cosine components including partial sign changes should appear in the frequency domain as sketched by the blue arrows.

$$(8) \quad T_{60\text{kts}}^{9001} = \begin{bmatrix} -0.0045 & -0.0030 & 0.0038 & 0.0027 \\ 0.0031 & -0.0043 & -0.0026 & 0.0034 \\ -0.0098 & -0.0026 & 0.0093 & 0.0020 \\ 0.0041 & -0.0097 & -0.0025 & 0.0068 \\ 0.0042 & 0.0129 & -0.0038 & -0.0111 \\ -0.0123 & 0.0047 & 0.0116 & -0.0034 \end{bmatrix}$$

Nevertheless, these differences can typically not be exploited due to limited control authority and are therefore discarded by setting up the T-matrix by elimination of related blade dissimilarities with symmetrizing – leading to rank-deficiency and to redundancy in the control inputs see [12] and [13]. In order to eliminate the redundancy, two approaches seem straight forward with the second one being selected:

- To select a reference blade and to set the control input of the reference blade to zero (typical approach for rotor tracking)
- To transform the control input vector into multi-blade coordinates and to eliminate the collective control input mode

In addition to other constraints, interaction with other control systems (namely pilot control, primary flight control and secondary flight control such as active vibration suppression, noise reduction and lead-lag damping enhancement) has to be avoided. The latter is guaranteed by a frequency domain splitting of the control variables and the use of quasi-steady flap deflections for in-flight tracking. The in-flight tracking control, which block diagram is presented in Figure 6, comprises a fast sampling signal processing subsystem (DFT) and slow sampling optimal correction estimation for the TEF consisting in:

- Signal processing block: Calculation of 1/rev and 2/rev feedback signal components from time history by DFT
- Inverted T-matrix of nominal plant quasi-steady behavior for calculation of corrective actions
- Gain block for feedback adjustment in terms of controller performance and robustness
- Controller integrator block including authority limitation functionality

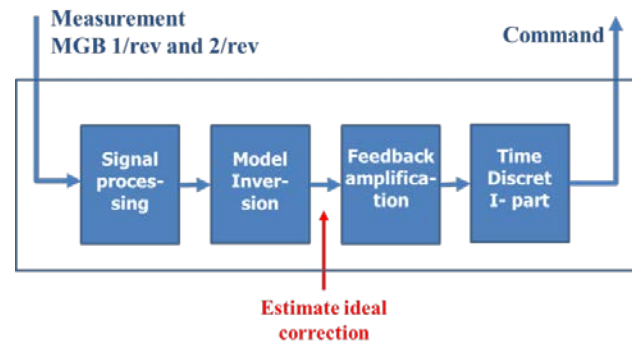


Figure 6: Block diagram of tracking controller

Several major contributions have been required to achieve a successful in-flight tracking. First an experimental transfer matrix identification regarding the 1/rev and 2/rev frequency, using flight-test data of a full-scale EC145 helicopter has been performed in order to validate the choice of the linear quasi-steady modeling and symmetrized transfer matrices within the TMA. For this purpose, constant control inputs of varying amplitudes were applied for the blades, shown in an exemplary manner in Figure 7. Each gradient of the regression lines for the various acceleration components and blades provides an entry into the transfer matrix.

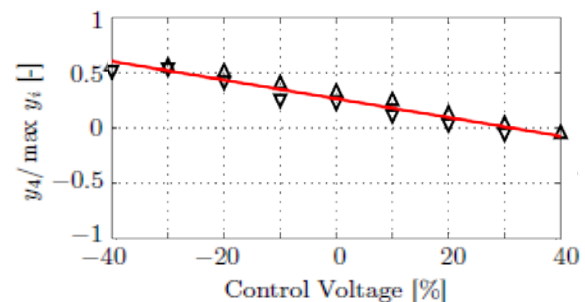


Figure 7: Normalized MGB acceleration component vs control, flight test and regression, see also [12]

In addition, the level of symmetry of these results can be assessed by compiling the results into polar diagrams with amplitudes reflected by length and phases mapped to angles, see Figure 8 for two different plants. A perfect rotor behavior is characterized by a perfect cross whereas dissimilarities in the control matrix might be based on different gains i.e. different lengths and on phase delays i.e. different rotation angles.

Second, closed-loop flight tests were carried out to study the ability of the automatic tracking control system under real conditions. An exemplary result of the flight tests is illustrated in Figure 9. Compared to the uncontrolled artificially disturbed reference data (blue) the automatic in-flight tracking system is able to substantially reduce the shown 1/rev vibration amplitude (red) from more than 80% at the gearbox.

Concerning the perceived reduction level in the cabin, similar results were confirmed by the flight crew.

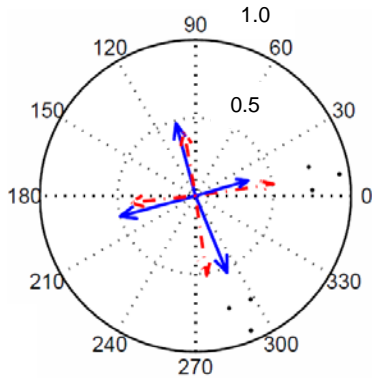


Figure 8: Normalized 1/rev transfer model parameters in Y direction: Amplitude and phase representation, flight test results, see also [12]

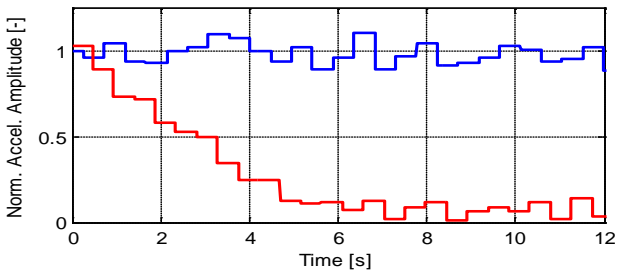


Figure 9: Normalized acceleration at 1/rev in Z direction: Uncontrolled blue, controlled red

In addition, Figure 10 illustrates the acceleration data in the frequency range 0.75rev to 2.25rev from flight-test experiments for the combined active in-flight tracking controller, comparing it with the acceleration data without an in-flight tracking system. The combined control system minimizes accelerations at frequency 1rev by more than 80% in x directions (same levels are also reached in y and z). Furthermore, the proposed algorithm significantly reduces the 2rev components by more than 90%. Regarding only the 1rev acceleration, the performance of the combined control concept and the pure 1rev controller is comparable in the presence of disturbances. Whereas the pure 1rev control system is limited to the rotational frequency of the main rotor, the combined concept reduces on top the 2rev accelerations resulting in a significant improvement of the typical so called low frequency vibration.

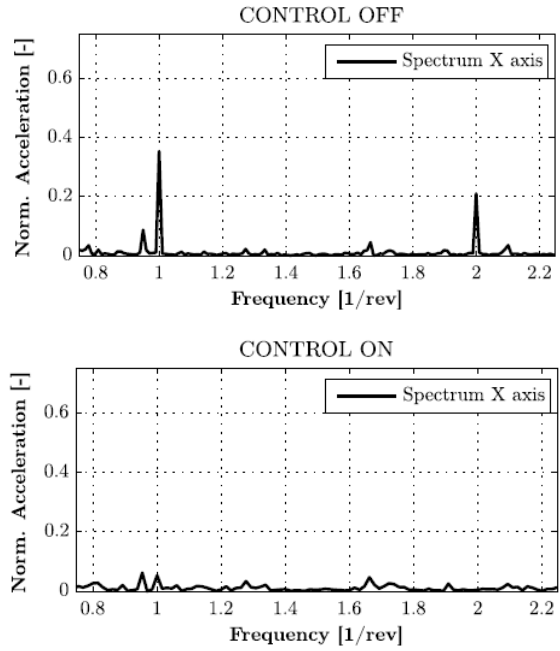


Figure 10: Spectral vibration in X direction during combined 1/rev & 2/rev in-flight tracking control

Finally, the robustness of the control algorithm has been demonstrated over the flight envelope. Similar to the vibration suppression, whereas the open loop identification has been performed by one flight regime, the possible evolution of the transfer behaviors over the flight conditions does not affect significantly the controller. It adapts automatically to reach the best performances. Figure 11 compares the 1rev lateral gear box vibration with and without in-flight tracking control over speed. It can be noticed, that on the one hand, the reference vibration without control increase non-linearly with the air velocity as expected, and on the other hand, the controlled vibration stays at an almost constant level. Without any gain scheduling, the in-flight tracking achieved over all conditions a minimal constant vibration level. This new function represents an outstanding step forward in terms of comfort over the whole flight envelope, but also DMC since tracking maintenance actions could be alleviated.

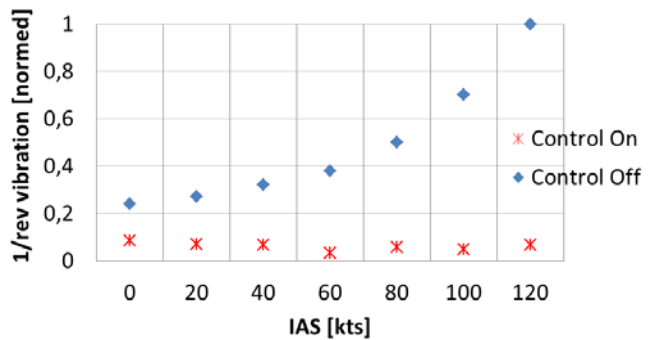


Figure 11: Normalized gear box lateral 1/rev vibration over speed

4. STABILITY ENHANCEMENT

For soft in-plane main rotors – the typical dynamic layout for today's rotorcrafts – the related low frequency of the rotor first regressive lagging mode might coalesce with the coupled airframe/rotor flap/roll modes in an adverse manner. This phenomenon is called air resonance for a helicopter in flight conditions. The pilot notices approaching the air resonance stability boundary by increasing low frequency roll motions due to loss of damping of the related coupled mode. In addition to worsened handling qualities and passenger comfort, this resonance can lead to high rotor loads and in the extreme catastrophic case to loss of integrity of the helicopter structure if the main rotor has insufficient in-plane damping.

Passive as well as active approaches can be used to avoid the air resonance phenomenon. Passive approaches focus on increasing the blade lead-lag damping with the help of, lag dampers; e.g. mechanical viscoelastic, hydro-elastic or hydraulic damper devices. Unfortunately, such concepts incur on the one hand both high recurring and maintenance costs and on the other hand generate significant loads especially with respect to the forced response of the first harmonic. Therefore, other solutions have been widely investigated.

Two main control approaches exist to enhance the stability properties of the coupled rotor/fuselage system. The first approach consists of feedback of rotorcraft roll and pitch rates to the actuators and is typically referred to as stability augmentation system (SAS) in the context of automatic flight control systems, [14, 15]. Related experience of AIRBUS HELICOPTERS for air resonance stabilization dates back to [16, 17] presenting flight test results of a modified Super Puma Mk2, which exploits actuators in the conventional flight control stabilization for feedback control of air resonance. Analytical studies in [18, 19] based on a four-blade hingeless BO105 demonstrator suggest that this solution is not suited for the control of air resonance for the investigated cases and led to poor performances in simulations.

In the second approach, rotor blade information is fed back in a control system commonly called individual blade control (IBC), see e.g. [20]. The approach is to increase lead-lag damping by using out-of-plane aerodynamics and Coriolis forces preferring feedback from rotor information. However, in the classical i.e. strong sense of IBC, the control loops are considered independently, whereas the particular mode shape of the first regressive lagging mode can only be observed efficiently when considering the rotor as a whole, applying multi-blade coordinates. Rotor state feedback cannot be implemented in most practical cases if no measurements are provided within the rotating frame

to reconstruct the rotor states, while these states are not always observable using sensors situated within the fuselage, [21]. Above all, no flight-tested proof of concept was performed in these studies.

A combined control path consists of adding the motions of the blades to the feedback loops of the SAS and is known as optimal control. In practice, however, this approach reveals itself to be difficult if the rotor states related to the lagging motion are not observable with sensors located in the fuselage. For such cases, a partial feedback of the states can lead to degraded performances of the stability enhancement, [21].

In light of the results of previous studies, the approach deployed for stability enhancement considers a control strategy based on IBC, i.e., measurements and control located on the blades in order to enhance the blade lag damping. System analysis studies using different key figures such as observability measures of Litz, Lueckel and Benniger confirms this approach. Figure 12 shows a comparison between rate feedback (top figure) and blade moment feedback (bottom figure) based on singular values. While controller design by rate feedback is complicated by an anti-resonance at frequencies of interest, see outlined box, the peak in case of blade moment feedback is considered as adequately suited for control purposes.

However, when classical IBC refers to separate control loops, the particular mode shape of the first regressive lagging mode suggests it makes more sense to consider the rotor as a whole entity. Because of the particular mode shape of the first lagging rotor mode at the frequency ω_c , the center of gravity of the rotor orbits around the axis of rotation at the frequency $|\Omega - \omega_c|$ in the fixed frame. The controller design accounts for this fact in a time-periodic control strategy based on the MBC transformation that targets the first regressive lagging mode specifically. In the isolated blade framework indeed, this mode is difficult to visualize. For instance, the first regressive lead-lag mode shape can be described using blade lead-lag motion as:

$$(9) \quad \zeta_{IBC}(t) = \begin{bmatrix} \zeta_1(t) = \zeta_0 \cdot \sin(\omega_r t) \\ \zeta_1(t) = \zeta_0 \cdot \sin\left(\omega_r t - \frac{\pi}{2}\right) \\ \zeta_1(t) = \zeta_0 \cdot \sin(\omega_r t - \pi) \\ \zeta_1(t) = \zeta_0 \cdot \sin\left(\omega_r t - \frac{3\pi}{2}\right) \end{bmatrix}$$

where the regressive mode description at the frequency $\omega_{c,reg} = |\Omega - \omega_c|$ does not explicitly appear.

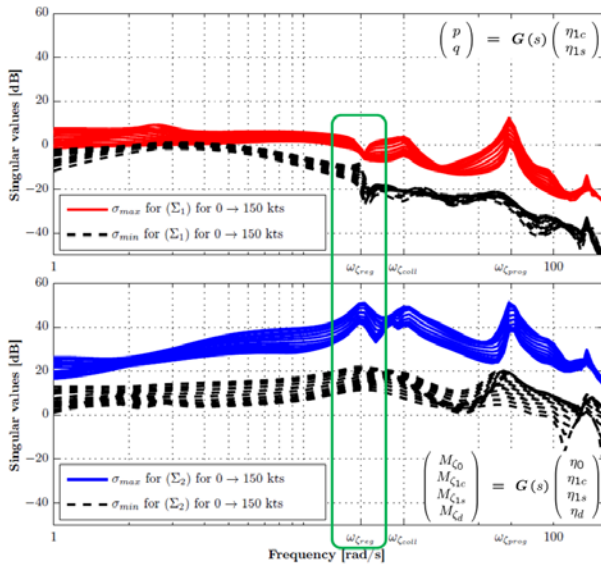


Figure 12: Singular value analysis: Rate feedback (top, anti-resonance close to $\zeta_{1,reg}$) and blade lag moment feedback (bottom, resonance close to $\zeta_{1,reg}$)

If we transform the mode shape ζ_{IBC} in multiblade coordinates by applying the transformation matrix $T_{i2m}(\Omega t)$ from blade coordinates to multi-blade coordinates, the mode shapes read

$$(10) \quad \begin{aligned} \zeta_{MBC}(t) &= T_{i2m}(\Omega t) \cdot \zeta_{IBC}(t) \\ &= \begin{bmatrix} \zeta_{coil}(t) = 0 \\ \zeta_{long}(t) = M \cdot \cos([\Omega - \omega_{\zeta}]t) \\ \zeta_{lat}(t) = M \cdot \sin([\Omega - \omega_{\zeta}]t) \\ \zeta_{diff}(t) = 0 \end{bmatrix} \end{aligned}$$

and the frequency of the first regressive lagging mode $\omega_{\zeta,reg} = |\Omega - \omega_{\zeta}|$ appears explicitly.

In order to capture the dynamic behavior of the rotorcraft demonstrators in the bandwidth of the air resonance phenomenon including specific features as the TEFs, an overall rotorcraft model main rotor plus airframe is required. The rotorcraft model used for controller design purposes is derived using the comprehensive rotorcraft analysis software CAMRAD II, [22]. The goal of the model is to accurately capture the dynamic behavior of the demonstrator rotorcrafts including specific features such as the TEFs in the bandwidth of the air resonance. The dynamic characteristics of the main rotor blades is described in CAMRAD II using the first five dynamic blade modes: first lagging ζ_1 and second lagging ζ_2 , first flapping β_1 and second flapping β_2 , and first torsional θ_1 modes. The inflow is modeled using a first-order representation according to Pit and Peters introducing three new states and yielding a low-frequency model of the wake influence in the rotor unsteady aerodynamic behaviour. The low-frequency rigid fuselage motion is modeled using the airframe velocities $[dx/dt, dy/dt, dz/dt]$ defined as

first-order states and the Euler angles $[\Phi, \Theta, \Psi]$. The elastic motion of the EC145 fuselage is described by using finite element results of NASTRAN resulting in the definition of five elastic airframe modes assessed to potentially impact dynamics at the frequency range of interest. Accounting for all the degrees of freedom, the numerical rotorcraft model is described by 62 first order states.

Model inputs are the TEF actuation commands $\eta = [\eta_0, \eta_{1c}, \eta_{1s}, \eta_d]^T$ defined in multi-blade coordinates, where the subscripts 0, 1c, 1s, and d indicates the collective, longitudinal and lateral cyclic, and differential forms. Outputs are the blade lagging moments $M_{\zeta} = [M_{\zeta 0}, M_{\zeta 1c}, M_{\zeta 1s}, M_{\zeta d}]^T$, defined in multi-blade coordinates as well; they are measured by strain gauges at the 0.12 R radial station of the rotor blades.

Because of the dependence of the aerodynamic loads on the azimuth $\psi = \Omega t$ of the blades, this rotorcraft model can be described for small perturbations by a Linear Time-Periodic (LTP) formulation [23, 24].

$$(11) \quad \begin{cases} \dot{x} = A(\psi)x + B(\psi)\eta \\ M_{\zeta} = C(\psi)x + D(\psi)\eta \end{cases} \quad \text{LTP}$$

where the state-space matrices are 2π periodic, and can be expanded in the Fourier series as

$$(12) \quad A(\psi) = A_0 + \sum_{n \neq 0} (A_{nc} \cos n\psi + A_{ns} \sin n\psi)$$

The time-periodic transformation from blade coordinates to multi-blade coordinates results in the projection of the relevant information present in the first harmonic of the system matrices onto the zeroth harmonic of the MBC matrices, [25]. Therefore, a linear time-invariant (LTI) model defined in MBCs accounts for significant parts of the periodic information relevant to the lead-lag mode dynamics, thus reducing interconnection errors induced by averaging the state-space matrices. Hence, it is preferred to define the model in an LTI-averaged formulation for controller design purposes:

$$(13) \quad \begin{cases} \dot{x} = A_0 x + B_0 \eta \\ M_{\zeta} = C_0 x + D_0 \eta \end{cases} \quad \text{LTI}$$

This open-loop identification of the model was restricted to the bandwidth of the first lagging mode in order to match accurately the behavior of the helicopter rotor in this frequency range. The model was tuned in terms of eigenvalues as well as the transfer behavior observed during the quasi-steady response of the blade moments to TEF excitation. The baseline frequency and damping results are compared to simulations in Figure 13. By changing specific parameters such as lag damping and stiffness in the numerical model, the dynamic characteristics of the lagging mode are tuned to

match flight-test data for the forward flight. This corresponds to the identification of relevant entries of the system matrix A_0 of the state space representation of Eq. (13).

The use of a LTI model for the controller design is justified by the linear behavior the TEFs input to the blade's lagging moments at the frequency of the first regressive lagging mode observed in open-loop flight tests and presented in Figure 14, where the cyclic lead-lag moment amplitudes $M_{\zeta_{1c}}$ and $M_{\zeta_{1s}}$ are linear with the input amplitude η , and the phases Φ_c and Φ_s are constant.

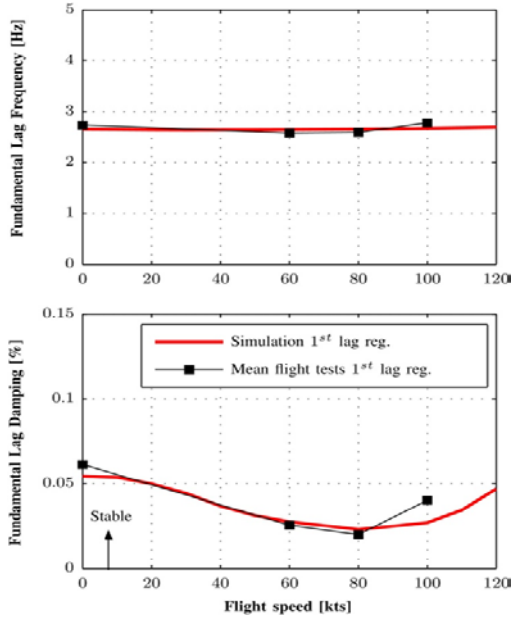


Figure 13: Regressive lead-lag frequency and damping: Flight test data versus simulation

The result of the model identification procedure is illustrated in Figure 15. The response of the lagging moments during the cyclic excitation of the first regressive lagging mode obtained in simulation is compared to the response of the demonstrator in flight conditions for 60 kts forward flight. The moments are scaled with $\|M_{\zeta}\|_{\infty} = \max(M_{\zeta, \text{sim}}, M_{\zeta, \text{FT}})$ defined as the maximum value of the moments from simulation $M_{\zeta, \text{sim}}$ and from flight test $M_{\zeta, \text{FT}}$. The agreement is excellent and constitutes an adequate basis for a model-based controller design.

The enhancement of the stability margins with respect to the air resonance phenomenon is assessed in this project by increasing the damping of the first regressive lagging mode instead of the inertial stability of the airframe. By reducing the amplitude of the source of the excitation of air resonance, a significant improvement of both the rotor and fuselage stability margins is expected. The requirements on the control performance are summarized qualitatively as follows. The controller shall:

- increase the damping of the first regressive lagging mode,
- avoid interaction with other dynamics,
- not interact with the pilot control in order to avoid impact on primary flight controls,
- be robust enough to cover the whole flight envelope and thus avoid gain scheduling,
- be simple and physically motivated.

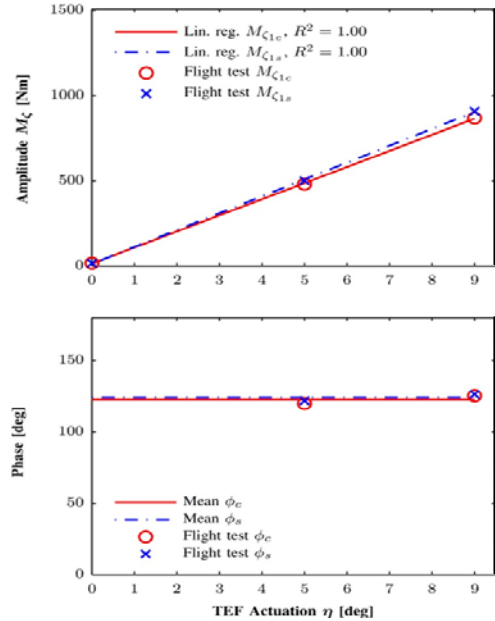


Figure 14: Linearity check of flight test lead-lag moments to TEFs input at $\zeta_{1, \text{reg}}$ frequency

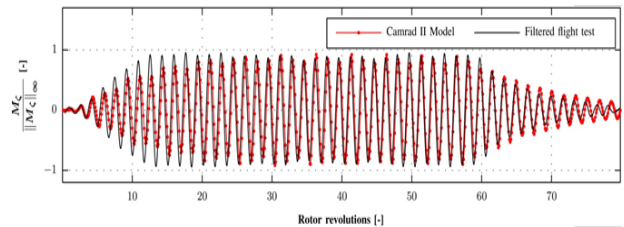


Figure 15: Time history of open-loop blade lead-lag moments during excitation: Flight test data versus simulation

The controller design refers to multi-blade coordinates in order to target the first regressive lagging mode specifically using the cyclic coordinates. In addition to differential input, collective input has little effect on air resonance as demonstrated by numerical means. Therefore, neither collective control nor differential control was used in the design described in this paper. The overall closed-loop scheme used in the flight is presented in Figure 16. The control scheme is composed of the following blocks:

- A gain g scales the IBC lagging moments M_{ζ} measured on the blade.

- A transformation block $T_{i2m}(\Omega t)$ transfers the signals of the blades into multi-blade coordinates. The transformation is computed in real-time during the flight tests using the time-varying rotor azimuth angle Ωt ,
- A bandpass (BP) filter acts as a washout filter and thus limiting the bandwidth of the controller to the vicinity of the targeted mode at $\omega_{\zeta,reg}$.

$$(14) \quad BP(s) = \left(\frac{2 \cdot \omega_{\zeta,reg} \cdot s}{(s + \omega_{\zeta,reg})^2} \right)^2$$

- A proportional-derivative (PD) filter adapts the phase of the signals to achieve a reduction of the output moments.

$$(15) \quad PD(s) = K_d \cdot \left(1 + \frac{T_d \cdot s}{1 + \frac{T_d}{N} \cdot s} \right)$$

- A transformation block $T^{-1}_{i2m}(\Omega t)$ transfers the signals from MBC back to the individual blades.
- A controller “on/off” switch ensures first a smooth start up over 2s to avoid nonlinear effects and second an abrupt stop allowing to observe free open- or closed-loop oscillations for damping and frequency measurements.

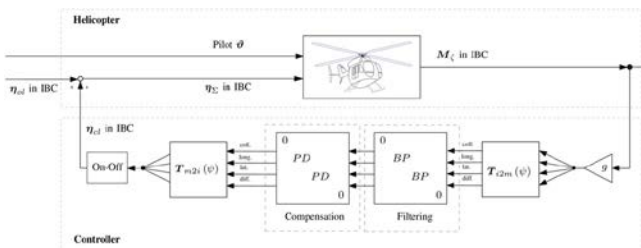


Figure 16: Controller structure for lead-lag damping enhancement [26]

While these controller elements are linked to functional aspects, safety issues were also considered during the design process as malfunctions of the controller might have the potential to significantly enhance the air resonance phenomenon. Related activities started with FMEA (failure mode and effect analysis) sketching the following steps:

- Define the functions of the closed-loop system
- Identify the potential failure(s) and estimate their severity
- Derive the potential effects of the failure and estimate their occurrence
- Estimate the detection capacity of the current detection means

- Evaluate the risks for each potential failure
- If necessary: provide to recommendations and perform actions

These activities resulted in the compilation of controller safety packages of different levels in order to monitor controller performance by analyzing input and output data streams. Regarding input data streams the following checks might be especially meaningful:

- Check outlier, ‘NaN’ and data blockage of measurements
- Check maximum input values (i.e. blade bending moments)
- Check coherence of measurements

In a similar manner, controller output checks can be performed – this time the measurements replaced by the output commands following a similar test logic.

The simulation presented in Figure 17 describes the root locus for the example of 100 kts forward flight. Through the combined action of the band-pass and proportional-derivative filters, the damping of the first regressive lagging mode $\zeta_{1,reg}$ can be increased from 4 to 15%. The other modes remain unchanged, except for the body flap/roll mode $\beta_{1,reg}/\Phi$ and the flap/pitch mode $\beta_{1,reg}/\theta$ as these modes are coupled with the blade lagging mode. The loss of damping of the coupled flap/body modes is caused by the damping transfer from the flap to the lag mode induced by the TEFs through the Coriolis forces.

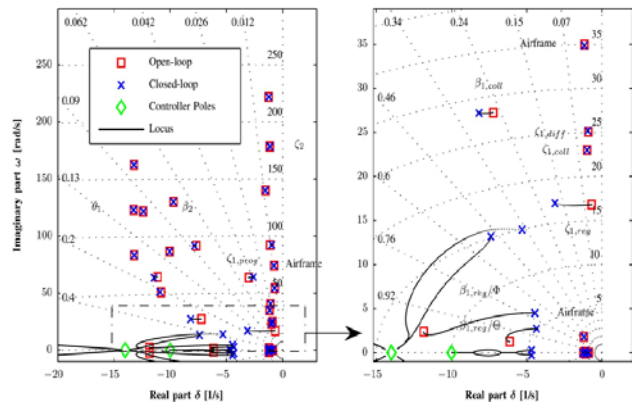


Figure 17: Root locus of the helicopter model at 100 kts level flight: Closed loop simulation results

The increased coupling of lag and flap dynamics induced by the controller is also visible in comparing the blade flap and lag bending moments as shown in Figure 18 using flight test data. Here uncoupled results are compared with different closed loop gains indicating increased levels of blade torsion and flap moments with increased controller power.

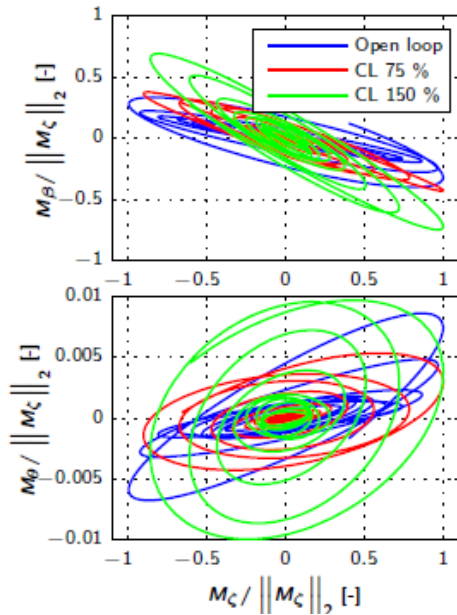


Figure 18: Analysis of free oscillations comparing flap and torsion moments versus lag moments: Flight test data, 80 kts

The loss of damping of the flap/body modes mentioned above can be accepted as the flap mode is provided with a great amount of aerodynamic damping. Nevertheless, an adequate compromise must be found in general in order not to decrease the damping of these modes too much e.g. in view of handling qualities. This trade-off was investigated in closed-loop by increasing gradually the gain from $0g_{nom}$ to $3g_{nom}$, and the behavior of the system was monitored with great attention. Time response of the rotor lagging moments and helicopter pitch and roll rates are presented in Figure 19 for 60 kts forward flight with controller gains $g = 1.5 g_{nom}$. The positive effect of the control is clearly visible in the quasi-steady response of the system during excitation, where a reduction of at least 30% of the lagging moments and airframe angular rates is achieved. Tuning capabilities of controller performance by adjusting the feedback gain is shown in Figure 20.

The signals measured after the end of the open-loop excitation are used for frequency and damping measurements in closed-loop presented in Figure 21. A strong increase of the damping of the first regressive lagging mode is achieved for all the tested flight conditions. Using a single controller without gain scheduling, the damping of the first regressive lagging mode is increased over three percentage points for flight speeds between hover and 80 kts demonstrating adequate robustness properties. The frequency remains almost constant, thus reducing side impact on the 1/rev blade loads.

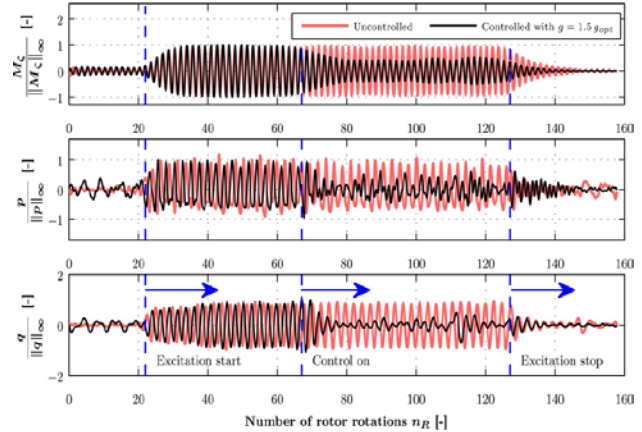


Figure 19: Time histories of filtered and normalized lag moments, roll, and pitch rates: Flight tests, 60 kts

The active damping enhancement using the TEFs, therefore, matches the performance of classical elastomeric dampers which typically add about three percentage points to the lead-lag damping for this size of helicopters.

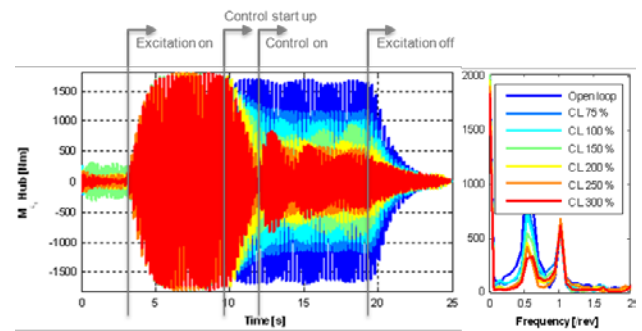


Figure 20: Time histories and spectral analysis of lag moments for controller gain variations: Flight test

5. CONCLUSIONS

This paper comprises the research activities performed during the last decade at AIRBUS HELICOPTERS on Blue Pulse active rotor control.

Blue Pulse active rotor control has demonstrated its multi-functionality including some world first in-flight demonstrations:

- ✓ Blue Pulse vibration suppression
- ✓ Blue Pulse noise cancellation
- ✓ Blue Pulse in-flight tracking
- ✓ Blue Pulse stability enhancement

In addition to advances in controller demonstration as shown in this paper, several key components of the active system have been boosted towards TRL6 [10], i.e.

- ✓ Miniaturized Electronics
- ✓ Active main rotor system
- ✓ Actuation units including piezo-driven TEFs

Besides, industrial challenges have been considered in a complementary manner [10], i.e.

- ☑ Overall weight neutrality
- ☑ Certifiability
- ☑ Serialisability
- ☑ Safety & reliability

In conclusions, Blue Pulse active rotor technology is considered to have achieved an adequate readiness level for being just around the corner.

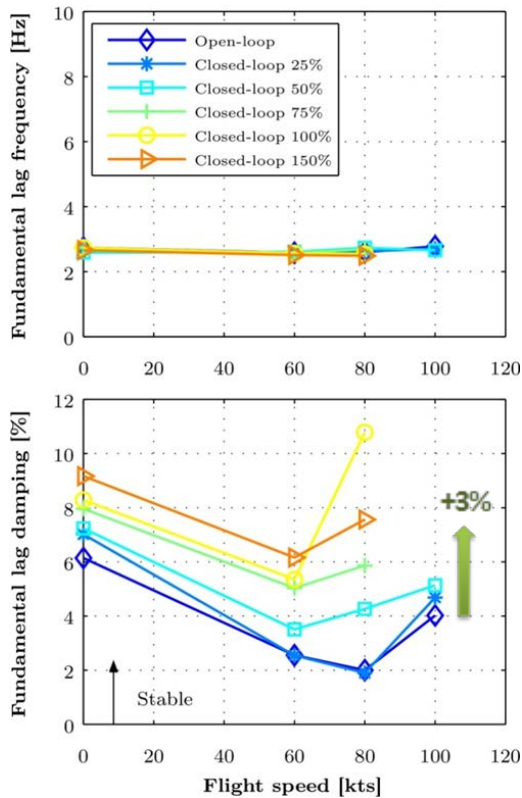


Figure 21: Regressive lead-lag frequency and damping for varying controller gains: Flight test results

ACKNOWLEDGEMENTS

Parts of this research have been performed in the frame of national research projects VAR and VAR2, supported by the BMWi. We are particularly thankful for the German support over the years. Besides we highly appreciate the very fruitful collaboration with our project partners AGI (formerly EADS Innovation Works) and Institute for Flight Mechanics and Control (University of Stuttgart).

NOTATION

- AGI Airbus Group Innovations (formerly EADS Innovation Works)
- BVI Blade Vortex Interaction
- DFT: Discrete Fourier Transform
- HHC: Higher Harmonic Control
- HIGE Hover In Ground Effect

- HOGE Hover Out of Ground Effect
- IAS Indicated Air Speed
- IBC Individual Blade Control
- KIAS Knots Indicated Air Speed
- LMS Least Mean Square
- MBC Multi-Blade Coordinates
- MIMO Multi Input Multi Output
- MGB Main Gear Box
- RPM Rotations Per Minute
- /rev Per Revolution
- SAS Stability Augmentation System
- SISO Single Input Single Output
- TAS True Air Speed
- TEF Trailing Edge Flap
- TMA Transfer Matrix Approach
- VIB Vibration
- ZF Friedrichshafen

REFERENCES

[1] Dieterich, O. et.al., “Trailing edge flaps for active rotor control - Aeroelastic characteristics of the ADASYS rotor system“, 62nd AHS Annual Forum, Phoenix, Arizona, 2006

[2] Ahci-Ezgi, E. et.al., “Piezo active rotor blade – Challenges and solutions“, 69th AHS Annual Forum, Phoenix, Arizona, 2013

[3] Konstanzer, P. et al., “Recent advances in Eurocopter’s passive and active vibration control“, 64th AHS Annual Forum, Montreal, Canada, 2008

[4] www.bluecopter.com

[5] Rauch, P., Gervais, M., Cranga, P., Baud, A., Hirsch, J-F., Walter, A., Beaumier, P., “Blue Edge™: The design, development and testing of a new blade concept“, 67th AHS Annual Forum, Virginia Beach, VA, May 2011

[6] Polychroniadis, M., Achache, M., “Higher harmonic control: Flight tests of an experimental system on SA349 research Gazelle“, 42nd AHS Annual Forum, Washington, 1986

[7] Roth, D., Enenkl, B., and Dieterich, O., “Active rotor control by flaps for vibration reduction, full scale demonstrator and first flight test results“, 32nd European Rotorcraft Forum, Maastricht, The Netherlands, Sept. 2006

[8] Dieterich, O. et al. “Model based H[∞] control for helicopter vibration reduction - Flight tests with active trailing edge flaps“, 33rd European Rotorcraft Forum, 2007

[9] Dieterich, O., “Application of modern control technology for advanced IBC systems“, 24th European Rotorcraft Forum, Marseille, France, 1998

[10] Rabourdin, A. et.al., “Blue Pulse active rotor control at Airbus Helicopters – New EC145 demonstrator & flight test results“, 70th AHS Annual

Forum, Montreal, Canada, May 2014

[11] Roth, D., "Advanced vibration reduction by IBC technology", 30th European Rotorcraft Annual Forum, Marseille France, Sept. 2004

[12] King F.A. et.al., "Performance characteristics of symmetrized in-flight tracking control", 70th AHS Annual Forum, Montreal, Canada, 2014

[13] King F.A. et.al., "In-flight rotor blade tracking control for helicopters using active trailing-edge flaps", AIAA Journal, 2014

[14] Panda, B., Mychalowycz, E., and Kothmann, B., "Active controller for Commanche air resonance stability augmentation", 60th AHS Annual Forum, Baltimore, MD, June 1999

[15] Lantzsch, R., Wolfram, J., and Hammers, M., "Increasing handling qualities and flight control performance using an air resonance controller", 64th AHS Annual Forum, Montreal, April–May 2008

[16] Krysinski, T., "Active control of aeromechanical stability", Proceedings of the AGARD/SMP Specialists' Meeting on Advances in Rotorcraft Technology, Ottawa, May 1996

[17] Almeras, P., "Active control of aeromechanical stability applied by Eurocopter", 23rd European Rotorcraft Forum, Dresden, Germany, Sept. 1997

[18] Reichert, G., and Arnold, U., "Active control of helicopter ground and air resonance", 16th European Rotorcraft Forum, Glasgow, Scotland, U.K., Sept. 1990

[19] Tettenborn, G., Kessler, C., and Reichert, G., "Comparison of IBC with active controllers using a conventional swashplate to suppress ground resonance", 23rd European Rotorcraft Forum, Dresden, Germany, Sept. 1997

[20] Ham, N. D., "Helicopter individual-blade-control research at MIT 1977–1985", 12nd European Rotorcraft Forum, Garmisch-Partenkirchen, Germany, Sept. 1986

[21] Takahashi, M. D., and Friedmann, P. P., "Design of a simple active controller to suppress helicopter air resonance", 44th AHS Annual Forum, Washington, D.C., June 1988

[22] Johnson, W., "A comprehensive analytical model of rotorcraft aerodynamics and dynamics", Theory Manual, Johnson Aeronautics, Palo Alto, CA, 1996

[23] Maurice, J.-B. et al., "Robust stability analysis of a linear time-periodic active helicopter rotor", Journal of Guidance, Control, and Dynamics", 35, 5, pp. 1625-1636, 2012

[24] Maurice J.-B. et al., "Floquet convergence analysis for periodic active rotor systems equipped

with trailing edge flaps", 35th European Rotorcraft Forum, Hamburg, Germany, 2009

[25] Hohenemser, K. H., and Yin, S.-Y., "Some application of the method of multiblade coordinates", Journal of the American Helicopter Society, Vol. 17, No. 4, 1972, pp. 3–12

[26] Maurice, J.-B., "Linear time-periodic control of helicopter air resonance", ISBN 978-3-8440-3085-3, published by Shaker